Frequency analysis of temperature-dependent interferometric signal for the measurement of the temperature coefficient of refractive index

Jianqin Zhou,[1,a)] Jun Shen,[1] and W. Stuart Neill[2]
[1]*Energy, Mining and Environment Portfolio, National Research Council of Canada, 4250 Wesbrook Mall, Vancouver, British Columbia V6T 1W5, Canada*
[2]*Energy, Mining and Environment Portfolio, National Research Council of Canada, 1200 Montreal Rd., Ottawa, Ontario K1A 0R6, Canada*

(Received 1 February 2016; accepted 25 June 2016; published online 19 July 2016)

A method of frequency analysis for the measurement of the temperature coefficient of refractive index (dn/dT) using a Fabry–Perot interferometer was developed and tested against ethanol and water. The temperature-dependent interferometric signal described by Airy's formula was analyzed in both the temperature and frequency domains. By fast Fourier transform, a low-pass filter was designed and employed to eliminate the noise superimposed on the signal. dn/dT was determined accurately from the noise-removed signal by peak analysis. Furthermore, the signal frequency parameters may be utilized for the material thermophysical property characterization. This method lays the foundation for an online dn/dT instrument for monitoring chemical processes. [http://dx.doi.org/10.1063/1.4958820]

I. INTRODUCTION

The temperature coefficient of refractive index (dn/dT) is an important parameter for material thermophysical property characterization. For example, dn/dT may be used to evaluate hydrocarbon fuel quality. It was reported that dn/dT can be utilized to discriminate biodiesels produced by transesterification using ethanol and methanol.[1] A recent study[2] on refinery streams revealed that dn/dT is clearly correlated to several important fuel properties. The refinery streams with a lower cetane number, lower distillation temperatures (T50, T90), and lower viscosity had a higher $-dn/dT$ value. Correlations of $-dn/dT$ with distillation temperatures and viscosity can be attributed to the dependence of this property on molecular size (or weight).[2,3]

Several methods, such as optical interferometer technique,[4,5] thermal lens spectrometry,[6,7] and minimum deviation method,[8] can be used for dn/dT measurement. Optical interferometer is a low-cost and easy-to-perform technique and has been widely applied.[2–5] It includes a heating device that induces a slow and uniform temperature variation in a sample, causing the intensity of interference fringe to change. The intensity is recorded against temperature as a temperature-dependent interferometric signal. In peak analysis, each temperature T corresponding to a signal peak is extracted and assigned with an interference order m to attain an m-T curve and its derivative, dm/dT, from which dn/dT can be deduced. In practice, the recorded interferometric signal is affected by noise, such as air turbulence, environmental vibration, or instrument noise. This leads to false peaks in the signal and thus error data in the m-T curve and dm/dT. Decreasing signal sampling rate may reduce signal false peaks.[3,5] However, because the noise was randomly distributed, a manual false peak removal was often required even at lower sampling rate.

To remove the noise from the signal, in this work, a method of frequency analysis was developed and tested against ethanol and water. By fast Fourier transform (FFT), a low-pass filter could be designed and employed to eliminate the noise superimposed on the signal. From the noise-removed signal, dn/dT values could be acquired accurately by peak analysis. Furthermore, the frequency parameters derived from the frequency analysis could be used for the material thermophysical property characterization.

II. OPTICAL INTERFEROMETER TECHNIQUE

Fig. 1 shows the principle of a Fabry–Perot interferometer and a schematic diagram of the experimental setup for dn/dT measurement. The sample to be measured can be gas, liquid, or transparent solid material. The solid material can be made as a plate with two parallel surfaces, while gas or liquid material can be enclosed in a transparent quartz cuvette with two parallel inner faces to form a plate. When a laser light is incident on the transparent plate, multiple reflections from the plate surfaces can create a multiple-beam interference fringe pattern described by Airy's formula,[9]

$$I_r = \frac{4R\sin^2(\delta/2)}{(1-R)^2 + 4R\sin^2(\delta/2)} I_i, \tag{1}$$

$$\delta = \frac{2\pi}{\lambda}\Delta s, \tag{2}$$

where λ is the wavelength of the laser light. I_i and I_r are the intensities of incident and reflected laser beams, respectively. R is the average reflectivity of the two parallel surfaces. δ is the phase difference induced by the difference of optical path length,

$$\Delta s = 2n(\lambda,T)\,L\cos\theta \cong 2n(\lambda,T)\,L\,(\theta < 1^\circ). \tag{3}$$

a)Author to whom correspondence should be addressed. Electronic mail: jianqin.zhou@nrc-cnrc.gc.ca. Fax: +1 604 221 3001.

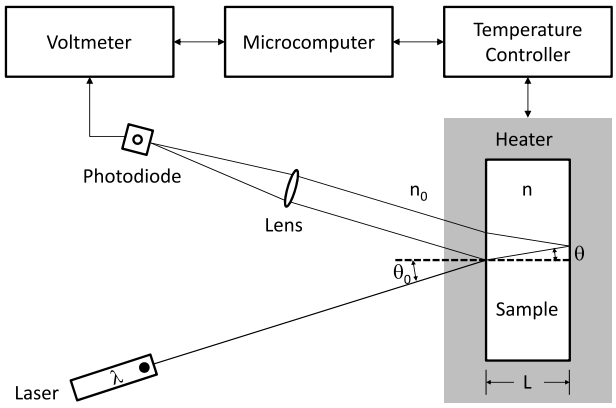

FIG. 1. The principle of a Fabry-Perot interferometer and a schematic diagram of the experimental setup for dn/dT measurement.

Here L is the thickness of the plate, θ is the angle of refraction, and n is the refractive index of the material. For the convenience of discussion, the thermal expansion of solid material and the temperature effect of quartz cuvette containing gas or liquid material are not taken into consideration in Eq. (3) and will be discussed in detail in Section IV. For a given wavelength λ of the laser light, the refractive index of the material is a function of temperature T,

$$n(\lambda, T) = n(T). \tag{4}$$

Defining the order of interference

$$m(T) = \frac{\delta}{2\pi} = \frac{\Delta s}{\lambda} = \frac{2L}{\lambda} n(T), \tag{5}$$

Eq. (1) can be expressed as

$$I_r(T) = \frac{F \sin^2 [m(T)\pi]}{1 + F \sin^2 [m(T)\pi]} I_i, \tag{6}$$

where

$$F = \frac{4R}{(1-R)^2}. \tag{7}$$

In this work, to measure the fringe intensity $I_r(T)$ with a liquid material, the liquid sample was contained in a transparent quartz cuvette ($L = 10$ mm) with two parallel inner faces and irradiated by a weak He-Ne laser beam ($\lambda = 632.8$ nm). Multiple reflections at both inner surfaces of the cuvette created an interference fringe pattern. A slow and uniform temperature variation was induced in the sample by an in-house made resistive heater controlled by a LakeShore 340 temperature controller. The heating of the sample caused a change of interference fringe intensity, which was detected by a photodiode and measured by a voltmeter (Agilent 34401A 6½ Digit Multimeter) as a temperature-dependent interferometric signal $I_r(T)$. Generally speaking, samples with positive or negative dn/dT will cause the interference fringe to move in opposite directions, which can be utilized to determine the sign of dn/dT. In the experiment, a known sample (e.g., ethanol) was measured first to determine the moving direction of a sample with negative dn/dT. Liquid hydrocarbons usually possess negative dn/dT.[3]

III. INTERFEROMETRIC SIGNAL ANALYSIS

To explore the methodology for accurate dn/dT measurement, a finite discrete-temperature digital signal is generated to simulate the interferometric signal $I_r(T)$. The parameters of an N point temperature sequence are summarized in Table I,

$$T = T_0 + j\delta_T = T_0 + j\frac{T_N - T_0}{N} \quad (j = 0, 1, \ldots, N-1). \tag{8}$$

A typical interference order, to a first approximation, is a single-variable quadratic function of temperature,

$$m(T) = c + bT + {}^1\!/_2 aT^2 \quad (T_0 \le T < T_N). \tag{9}$$

For a normalized simulation signal generated by Eq. (6),

$$I(T) = \frac{I_r(T)}{I_i} = \frac{F \sin^2 [m(T)\pi]}{1 + F \sin^2 [m(T)\pi]} \quad (T_0 \le T < T_N), \tag{10}$$

the equation coefficients in Eq. (9) are chosen as $a = 0.1\ K^{-2}$, $b = 1.0\ K^{-1}$, and $c = -56.25$ to set $m(25\ ^\circ\text{C}) = 0$. The average reflectivity R is chosen as 0.1 and F is about 0.5 [Eq. (7)]. The generated simulation signal is shown in Fig. 2.

A. Signal analysis

The fringe intensity $I(T)$ described by Airy's formula can be transformed to its interference order $m(T)$ by peak analysis. Referring to Eq. (10) and Fig. 2, when $m(T)$ varies with temperature, the maxima of $I(T)$ will appear at half-integral values ($m = {}^1\!/_2, 1{}^1\!/_2, 2{}^1\!/_2, \ldots$) and minima at integral values $m = (1, 2, 3, \ldots)$. Therefore, by extracting the temperature values at the maxima and minima of $I(T)$ and assigning $m(T)$ to each temperature value, $I(T)$ can be transformed to $m(T)$.

Fig. 3(a) presents the transformed interference order $m(T)$, which can be fitted to Eq. (9) by least-squares curve fitting to obtain equation coefficients. Fig. 3(b) shows the first derivative of the interference order $m' = dm/dT$, which is very important in the following aspects:

1. dm/dT is equal to signal frequency f — the number of peaks or valleys per unit temperature (Fig. 2),

$$f = m'. \tag{11}$$

TABLE I. The parameters of an N point temperature sequence.

Temperature range			Sample number	Sample interval	Signal resolution	Highest frequency	Frequency resolution
T_0	T_N	$\Delta T = T_N - T_0$	N	$\delta_T = \Delta T / N$	$2\delta_T$	$1/2\delta_T$	$1/\Delta T$
25 °C	35 °C	10 °C	5000	0.002 °C	0.004 °C	250 K^{-1}	0.1 K^{-1}

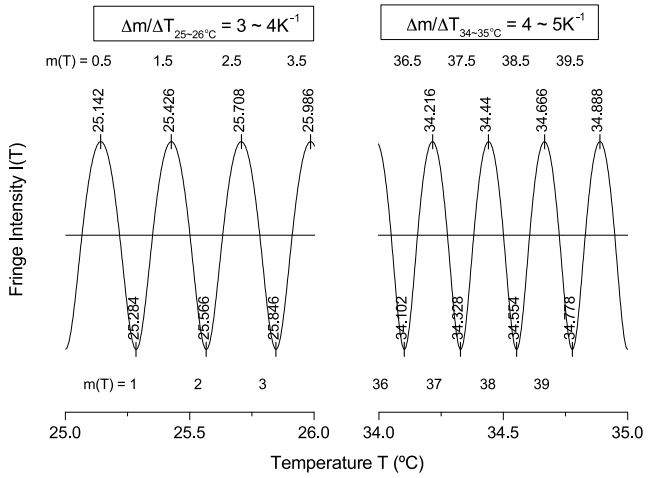

FIG. 2. The generated simulation signal $I(T)$. The interference order $m(T)$ is assigned to the temperature values at the maxima and minima of $I(T)$.

For the simulation signal [Eq. (9)], we have the signal frequency

$$f = m' = b + aT = 1 + 0.1T \quad (T_0 \le T < T_N), \tag{12}$$

the average frequency across the observation temperature range $(T_0 \le T < T_N)$

$$\overline{f} = \overline{m'} = b + a\overline{T} = b + a\frac{T_0 + T_N}{2} = 4K^{-1}, \tag{13}$$

and the frequency change across the observation temperature range $(T_0 \le T < T_N)$

$$\Delta f = \Delta m' = a\Delta T = a\,(T_N - T_0) = 1K^{-1}. \tag{14}$$

2. dm/dT is proportional to the temperature coefficient of refractive index dn/dT [Eq. (5)],

$$\frac{dn}{dT} = \frac{\lambda}{2L}m'. \tag{15}$$

Thus, dn/dT can be calculated. For the experimental setup, $\lambda = 632.8$ nm, $L = 10$ mm,

$$\frac{dn}{dT} = \left(0.3164 \times 10^{-4}\right)m'. \tag{16}$$

3. dm/dT is affected by limited sampling number of discrete signal and the noise in a practical measurement.

B. Noise analysis

Due to the limited sampling number, the peak/valley position of discrete signal may not be exactly the same as that of continuous signal (Fig. 4, $m = 0.5, 1, 1.5$), resulting in signal frequency variations (Table II).

Furthermore, the noise (air turbulence, environmental vibration, instrument noise, etc.) may distort the interferometric signal. As a result, the peak/valley position of the signal may be shifted (Fig. 5, $m = 0.5, 2.5$), causing signal frequency fluctuations; and the false peak/valley of the signal may be generated (Fig. 5, $m = 1, 1.5$), yielding signal false frequencies (Table II).

Shown in Table II, the false frequency is the major factor that will affect the measurement accuracy. Choosing a lower sampling rate may bring about more frequency variations (Fig. 6) and fluctuations (Fig. 7) but less false frequencies. Fig. 7 shows that, with given test conditions, a sampling rate below 500 sample/K was suitable for ethanol to avoid the false frequencies. However, it is time consuming to find an optimised sampling rate for different materials under different test conditions. Furthermore, because the noise was randomly distributed, a manual false frequency removal was often required even at lower sampling rate.

To reduce the frequency variations and fluctuations while eliminating the false frequencies, the frequency structures of the signal and noise have been analyzed and a methodology has been developed for accurate dn/dT measurement. With this methodology, a higher sampling rate is utilized to restrain the frequency variations and fluctuations, while an FFT low-pass filter is employed to block the false frequencies.

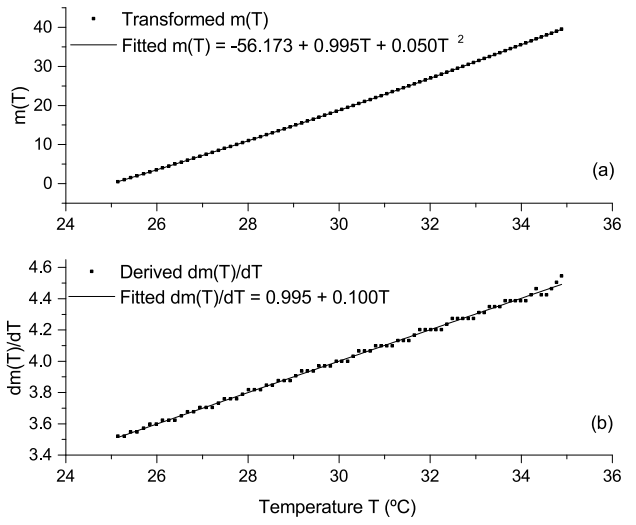

FIG. 3. The transformed $m(T)$ and its first derivative $dm(T)/dT$.

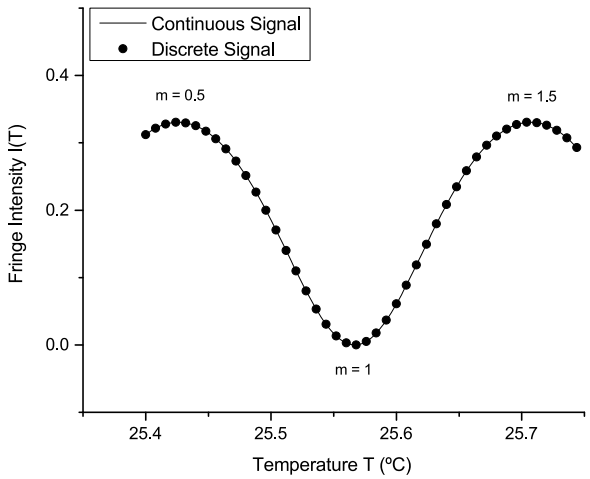

FIG. 4. Signal peak/valley position is affected by the limited sampling number.

TABLE II. Signal frequency change caused by the inaccurate peak/valley position and the false peak/valley information.

	Continuous signal			Discrete signal			Discrete signal + the noise				
m	0.5	1.0	1.5	0.5	1.0	1.5	0.5	1.0	1.5	2.0	2.5
T (°C)	25.426	25.567	25.707	25.424	25.568	25.704	25.432	25.528	25.544	25.568	25.696
f (K^{-1})		3.55	3.57		3.47	3.68		5.21	31.25	20.83	3.91

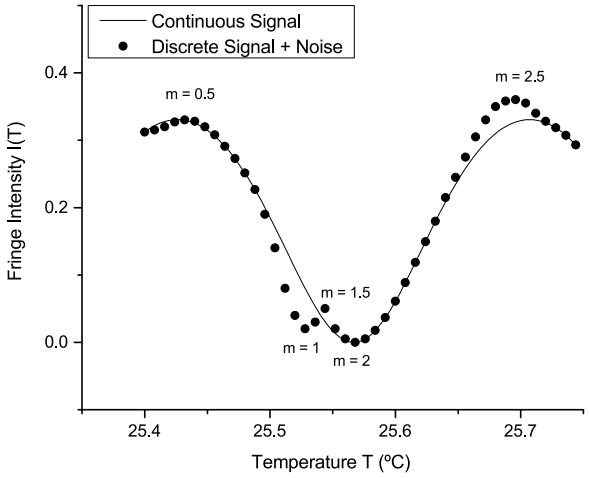

FIG. 5. Signal peak/valley position is affected by the noise.

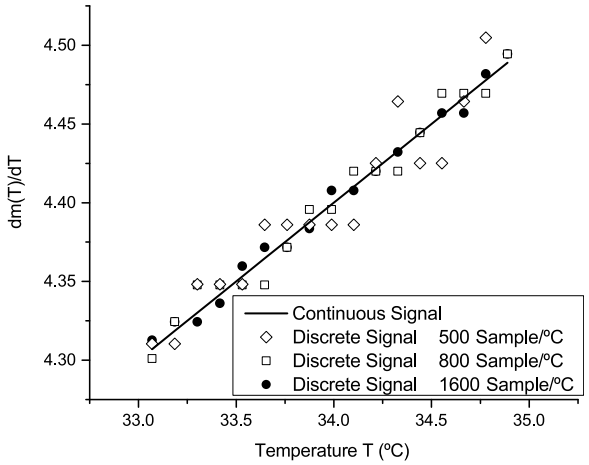

FIG. 6. Signal frequency ($f = m' = dm/dT$) derived from the simulation signal [Eq. (10)] at a different sampling rate. Lower sampling rate will bring about more frequency variations.

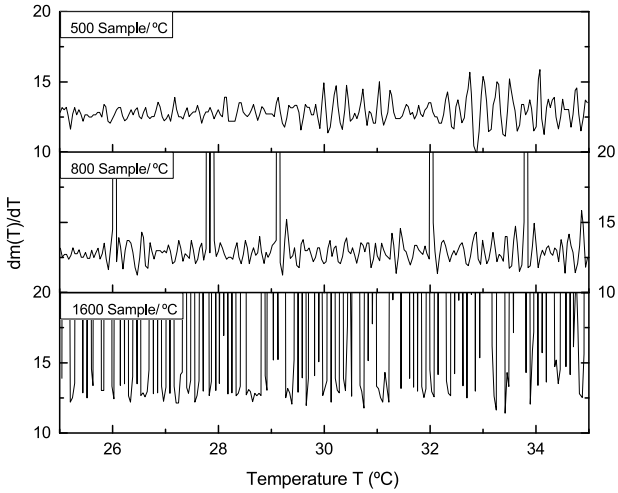

FIG. 7. Signal frequency ($f = m' = dm/dT$) derived from the measured signal (anhydrous ethanol) at a different sampling rate. Lower sampling rate will bring about more frequency fluctuations but less false frequencies.

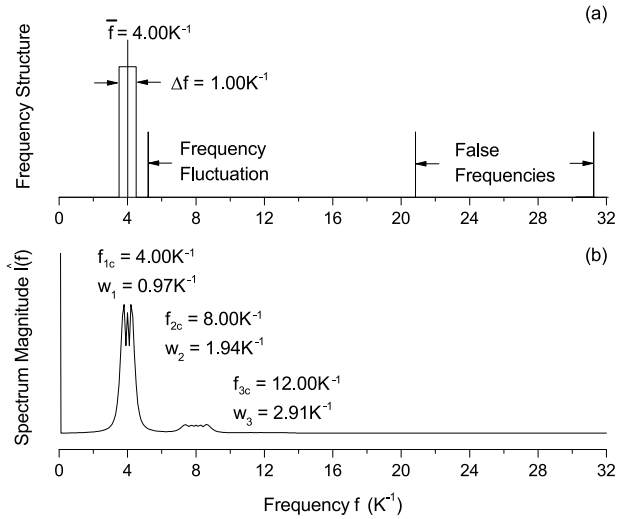

FIG. 8. (a) The frequency structures of simulation signal and noise. (b) The spectrum magnitude of the simulation signal obtained by FFT.

C. Frequency analysis

The frequency structures of the signal [Eq. (9)] and noise (Fig. 5) are shown in Fig. 8(a), in which the average frequency $\bar{f} = 4K^{-1}$ and the frequency change $\Delta f = 1K^{-1}$ [Eqs. (13) and (14)]. Some frequency fluctuations and all false frequencies (Table II) are higher than the maximum signal frequency $\bar{f} + \Delta f/2 = 4.5K^{-1}$.

The fringe intensity $I(T)$ described by Airy's formula can be transformed to its spectrum magnitude $\hat{I}(f) = \mathcal{F}[I(T)]$ by FFT[10] (Fig. 8(b)).

Fig. 8 shows that the average frequency is related to the center frequencies f_{qc} of the qth spectrum harmonic components,

$$\bar{f} \approx f_{1c} = f_{2c}/2 = f_{3c}/3 = f_{qc}/q = 4.00K^{-1}, \quad (17)$$

while the frequency change is related to the full width at half maximum (FWHM) w_q of the qth spectrum harmonic components,

$$\Delta f \approx w_1 = w_2/2 = w_3/3 = w_q/q = 0.97K^{-1}. \quad (18)$$

Fig. 9 and Table III provide more information about the relationship between the signal frequency structure and the signal spectrum magnitude obtained by FFT. With the decrease

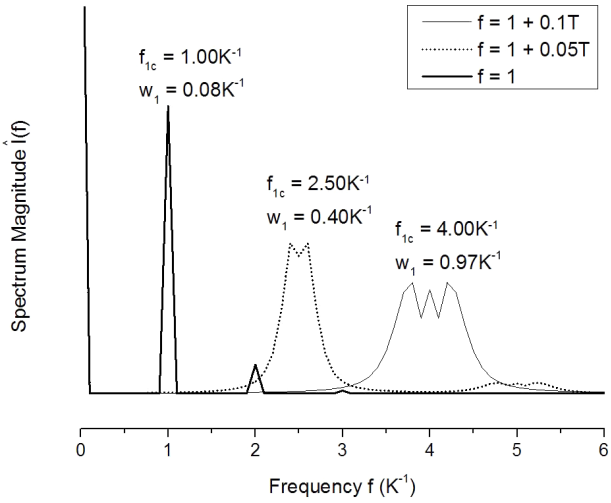

FIG. 9. The spectrum magnitude of the simulation signal with different simulation parameters $(a = 0, 0.05, 0.1K^{-2})$.

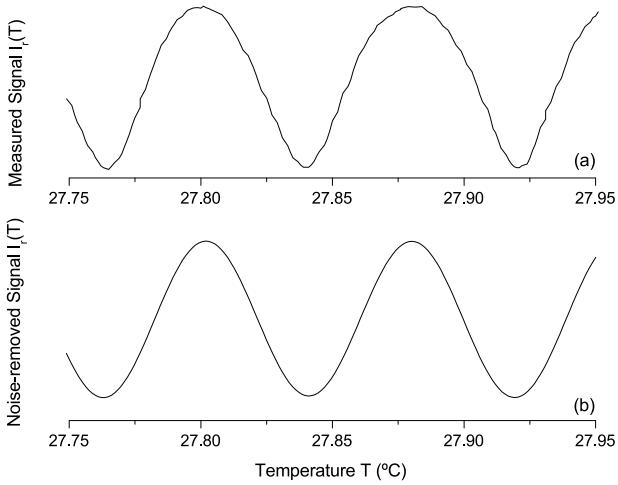

FIG. 10. (a) The interferometric signal $I_r(T)$ measured with ethanol. (b) The noise-removed signal $I_r(T)$.

of FWHM, the spectrum peak is getting sharper and dm/dT becomes a constant.

Based on the above discussion, it can be concluded that 1. the frequency structure of $I(T)$ is contained in the fundamental component of $\hat{I}(f)$. 2. Some frequency fluctuations and all false frequencies go beyond the fundamental component of $\hat{I}(f)$. 3. An FFT low-pass filter can be applied to $I(T)$ to keep the frequency structure but restrain frequency fluctuations and eliminate false frequencies. Consequently, a methodology for accurate dn/dT measurement can be summarized as follows: 1. apply FFT to transform $I(T)$ to $\hat{I}(f)$ and find f_{1c} and w_1 to determine the cutoff frequency of an FFT low-pass filter $(f_{cutoff} > f_{1c} + w_1/2)$. 2. Employ the filter to remove the noise from $I(T)$. 3. Perform peak analysis to derive dn/dT from the noise-removed $I(T)$.

IV. EXPERIMENTAL RESULTS AND DISCUSSION

The methodology for accurate dn/dT measurement was tested against anhydrous ethanol and de-ionized water. In the experiments, the signal sampling rate was 800 samples/°C and the observation temperature range was 25–35 °C.

The interferometric signals measured with ethanol and water are shown in Figs. 10(a) and 14(a); and the signal frequencies $f = dm(T)/dT$ derived from the measured signals $I_r(T)$ by peak analysis are shown in Figs. 11(a) and 15(a). The noise superimposed on the signal [Figs. 10(a) and 14(a)] brought about frequency fluctuations and false frequencies [Figs. 11(a) and 15(a)].

The signal spectrums $\hat{I}(f)$ transformed from the measured signals $I_r(T)$ by FFT are shown in Figs. 12 and 13. Comparing Fig. 12 with Fig. 13, the average frequency $(\overline{f} \approx f_{1c})$ of ethanol is higher than that of water and the frequency change $(\Delta f \approx w_1)$ of ethanol is smaller than that of water, indicating that the dn/dT of ethanol is large but nearly a constant, while that of water is small but more temperature dependent. By FFT low-pass filtering, the noise was removed thoroughly from the measured signals [Figs. 10(b) and 14(b)], and the frequency fluctuations were restrained and the false frequencies were blocked [Figs. 11(b) and 15(b)].

The experimental results are summarized in Table IV. The dn/dT values over the observation temperature range 25–35 °C may be found in the derived equations, and the measured data are in very good agreement with the literature values.[11] This agreement demonstrates that accurate results can be achieved with this method. Moreover, the standard deviations are only about 0.075% and 1.03% of the measured mean values of ethanol and water, respectively, exhibiting high precision.

Up to now, the thermal expansion of solid material and the temperature effect of quartz cuvette containing gas or liquid material have not been taken into consideration in Eq. (3). For an isotropic transparent solid with two parallel surfaces, considering the contribution of material thickness change to the interferometric signal, Eq. (3) can be expressed as

$$\Delta s = 2n(T)L(T), \tag{19}$$

$$f = \frac{dm}{dT} = \frac{d}{dT}\left(\frac{\Delta s}{\lambda}\right) = \frac{2}{\lambda}\left(L\frac{dn}{dT} + \frac{dL}{dT}n\right). \tag{20}$$

The thickness change of solid material due to the thermal expansion can be expressed as

$$\frac{dL}{dT} = \alpha L, \tag{21}$$

TABLE III. The center frequency and FWHM of spectrum fundamental component corresponding to different simulation parameters $(a = 0, 0.05, 0.1K^{-2})$.

T_0	T_N	ΔT	$\overline{T}$	b	a	$f = b + aT$	$\overline{f} = b + a\overline{T}$	f_{1c}	$\Delta f = a\Delta T$	w_1
					0.10 K^{-2}	$1.0 + 0.10T$	4.0 K^{-1}	4.0 K^{-1}	1.0 K^{-1}	0.97 K^{-1}
25 °C	35 °C	10 °C	30 °C	1 K^{-1}	0.05 K^{-2}	$1.0 + 0.05T$	2.5 K^{-1}	2.5 K^{-1}	0.5 K^{-1}	0.40 K^{-1}
					0	1.0 K^{-1}	1.0 K^{-1}	1.0 K^{-1}	0	0.08 K^{-1}

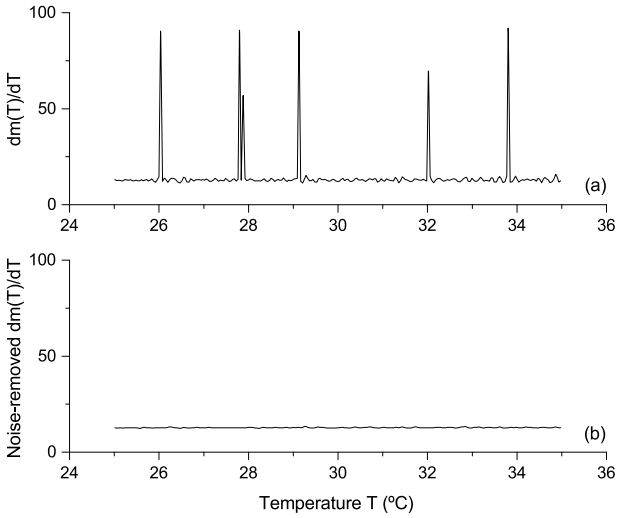

FIG. 11. (a) The signal frequency $dm(T)/dT$ derived from the interferometric signal $I_r(T)$ measured with ethanol. (b) The signal frequency $dm(T)/dT$ derived from the noise-removed signal $I_r(T)$.

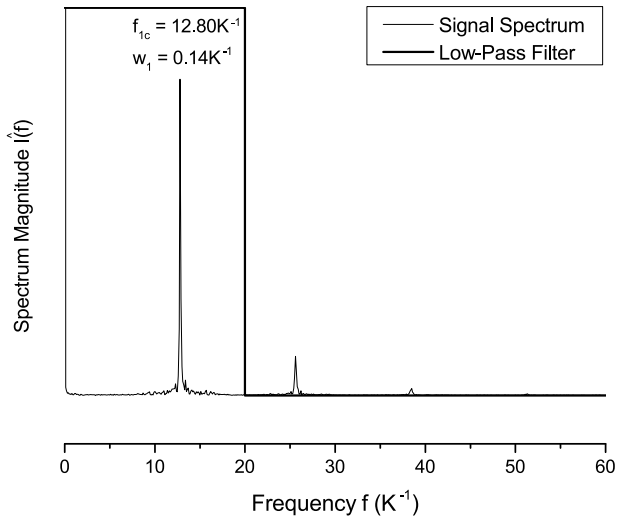

FIG. 12. The signal spectrum $\hat{I}(f)$ transformed from the interferometric signal $I_r(T)$ measured with ethanol.

where α is the linear thermal expansion coefficient, and we have

$$f = \frac{2L}{\lambda}\left(\frac{dn}{dT} + \alpha n\right). \tag{22}$$

The measured signal frequency contains the component contributed by sample refractive index change and that contributed by sample thickness change. Defining the temperature coefficient of optical path length

$$\frac{dS}{dT} = \frac{\lambda}{2L} f = \frac{dn}{dT} + \alpha n, \tag{23}$$

the measured signal frequency can be used for characterizing the thermophysical property of transparent solid materials, such as optical glasses, within a large observation temperature range.[5]

For the gas or liquid enclosed in a transparent quartz cuvette, the Fabry-Perot interferometer actually consists of three layers with four parallel surfaces (S_1, S_2, S_3, S_4): the

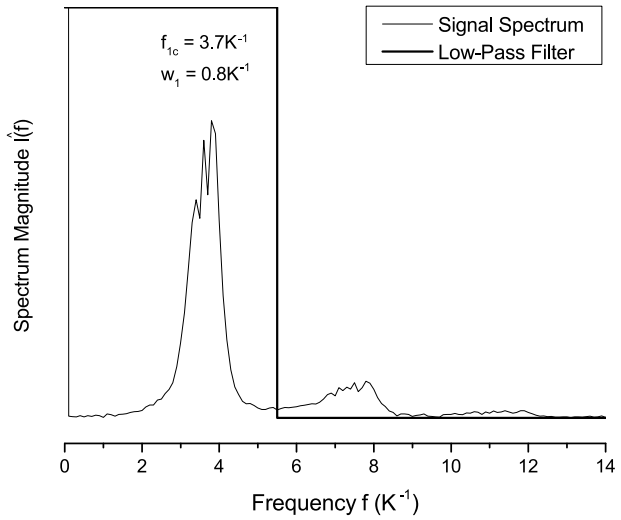

FIG. 13. The signal spectrum $\hat{I}(f)$ transformed from the interferometric signal $I_r(T)$ measured with water.

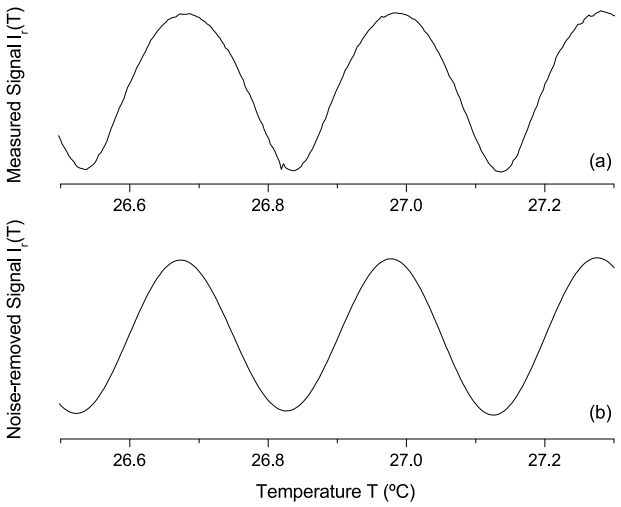

FIG. 14. (a) The interferometric signal $I_r(T)$ measured with water. (b) The noise-removed signal $I_r(T)$.

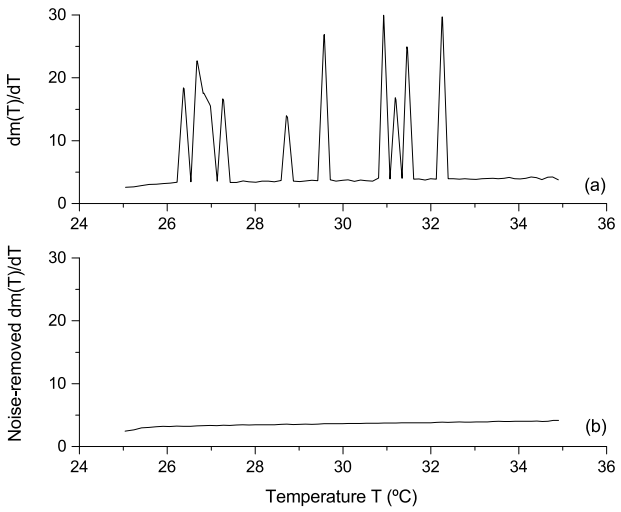

FIG. 15. (a) The signal frequency $dm(T)/dT$ derived from the interferometric signal $I_r(T)$ measured with water. (b) The signal frequency $dm(T)/dT$ derived from the noise-removed signal $I_r(T)$.

TABLE IV. Parameters for material thermophysical property characterization across the observation temperature range 25–35 °C.

	Frequency parameter (K^{-1})			$-dn/dT\,(\times 10^{-4}K^{-1})$		
Sample	$\bar{f} \approx f_{1c}$	$\Delta f \approx w_1$	$\Delta f/\bar{f}$	25 – 35 °C	25 °C[a]	25 °C (the literature)[b]
Ethanol	12.8	0.14	1.1%	3.90 + 0.005T	4.025 ± 0.003	4.02
Water	3.7	0.8	22%	0.12 + 0.034T	0.97 ± 0.01	0.99

[a]Mean value of ten measurements.
[b]Reference 11.

front cuvette wall (S_1–S_2), the sample in the cuvette (S_2–S_3), and the rear cuvette wall (S_3–S_4). The measured temperature-dependent interferometric signal can be considered as a superposition of six interferometric signals with different free spectral ranges (S_1–S_2, S_1–S_3, S_1–S_4, S_2–S_3, S_2–S_4, S_3–S_4), and Eq. (3) can be expressed as

$$\Delta s_{12} = 2\,(n_{Si} l)\,, \tag{24}$$
$$\Delta s_{13} = 2\,(n_{Si} l + nL)\,, \tag{25}$$
$$\Delta s_{14} = 2\,(n_{Si} l + nL + n_{Si} l)\,, \tag{26}$$
$$\Delta s_{23} = 2\,(nL)\,, \tag{27}$$
$$\Delta s_{24} = 2\,(nL + n_{Si} l)\,, \tag{28}$$
$$\Delta s_{34} = 2\,(n_{Si} l)\,. \tag{29}$$

Refer to Eqs. (20)–(22), these differences of optical path length generate six interferometric signals with different signal frequencies,

$$f_{12} = f_{\mathrm{Si}}, \tag{30}$$
$$f_{13} = f_{dn/dT} + f_{\mathrm{Si}}, \tag{31}$$
$$f_{14} = f_{dn/dT} + 2f_{\mathrm{Si}}, \tag{32}$$
$$f_{23} = f_{dn/dT}, \tag{33}$$
$$f_{24} = f_{dn/dT} + f_{\mathrm{Si}}, \tag{34}$$
$$f_{34} = f_{\mathrm{Si}}, \tag{35}$$
$$f_{dn/dT} = \frac{2L}{\lambda}\frac{dn}{dT}, \tag{36}$$
$$f_{\mathrm{Si}} = \frac{2l}{\lambda}\left(\frac{dn_{Si}}{dT} + \alpha_{Si} n_{Si}\right). \tag{37}$$

Here $l = 1$ mm, $n_{Si} = 1.46$, $dn_{Si}/dT = 1.01 \times 10^{-5}\ K^{-1}$, and $\alpha_{Si} = 1.83 \times 10^{-7}\ K^{-1}$ are the wall thickness, refractive index, temperature coefficient of refractive index, and linear thermal expansion coefficient of the fused-quartz cuvette, respectively.[12,13] $f_{dn/dT}$ is the frequency component contributed by sample refractive index change, while f_{Si} is the frequency component contributed by cuvette temperature effect. The ratio

$$\gamma = \frac{f_{\mathrm{Si}}}{f_{dn/dT}} = \frac{l}{L}\frac{\frac{dn_{Si}}{dT} + \alpha_{Si} n_{Si}}{\frac{dn}{dT}} = \frac{1}{10}\frac{1.01 \times 10^{-5} + 2.67 \times 10^{-7}}{|dn/dT|} = \frac{1.04}{|dn/dT| \times 10^4}\%. \tag{38}$$

In the case of distilled water, $dn/dT = -0.99 \times 10^{-4}\ K^{-1}$ and $\gamma = 1.05\%$. Most liquid samples have higher $|dn/dT|$ values than distilled water. For example, in the case of ethanol, $dn/dT = -4.02 \times 10^{-4}\ K^{-1}$ and $\gamma = 0.26\%$. The cuvette is designed to have thin walls ($l = 1$ mm) but a thick sample ($L = 10$ mm) for minimizing its temperature effect on the interferometric signal. $f_{12} = f_{34} = f_{\mathrm{Si}}$ is almost a DC signal and will not affect the peak analysis accuracy, while f_{13}, f_{14}, and f_{24} may cause some negligible frequency shift from $f_{23} = f_{dn/dT}$; thus, the measured signal frequency is

$$f \cong f_{dn/dT} = \frac{2L}{\lambda}\frac{dn}{dT}. \tag{39}$$

Since the signal frequency is associated with the change of optical path length [Eq. (20)], it is convenient to analyse the temperature-dependent interferometric signals in frequency domain and investigate the frequency components contributed by the different factors, such as sample refractive index change, sample thermal expansion, and cuvette temperature effect.

For transparent solid material, the signal frequency is associated with the temperature coefficient of optical path length [Eq. (23)], while for gas or liquid material, the signal frequency is associated with the temperature coefficient of refractive index [Eq. (39)]. Therefore, it is convenient to utilize signal frequency parameters to characterize material thermophysical property. Furthermore, by real-time FFT, the signal frequency and thus the material dS/dT or dn/dT can be acquired instantly, which will be presented in a later work. The methodology described in this paper may be used to build an instrument to monitor changes in the thermophysical property of process materials. It is envisioned that this instrument may have value for process control applications or quality control inspections.

V. CONCLUSION

The method of frequency analysis for dn/dT measurement has been developed and tested for ethanol and water. For accurate and precise dn/dT measurements, frequency analysis needs to be performed before conducting peak analysis to remove the noise from the measured interferometric signal. By FFT, a low-pass filter can be designed and employed to restrain frequency fluctuations and eliminate false frequencies. The experimental results show that the method can work at any sampling rate with different materials. The signal processing is simple, the noise reduction is effective, and the measured data are accurate and precise across the observation temperature range. With the method developed in this work, we are able to examine material interferometric signal from another perspective and characterize material thermophysical property with signal frequency parameters. The method lays the foundation for real-time monitoring or process control using dn/dT measurement.

ACKNOWLEDGMENTS

Financial support from the Government of Canada's ecoENERGY Innovation Initiative (ecoEII), Project No. EETR-015, is gratefully acknowledged.

[1]M. P. P. Castro, A. A. Andrade, R. W. A. Franco, P. C. M. L. Miranda, M. Sthel, H. Vargas, R. Constantino, and M. L. Baesso, Chem. Phys. Lett. **411**, 18 (2005).
[2]J. Shen, N. G. C. Astrath, P. R. B. Pedreira, F. B. Guimarães, R. Gieleciak, Q. Wen, K. H. Michaelian, C. Fairbridge, L. C. Malacarne, J. H. Rohling, and M. L. Baesso, Fuel **163**, 324 (2016).
[3]Q. Wen, J. Shen, Z. Shi, E. Dy, K. H. Michaelian, C. Fairbridge, N. G. C. Astrath, J. H. Rohling, and M. L. Baesso, Chem. Phys. Lett. **539**, 54 (2012).
[4]T. Y. Fan and J. L. Daneu, Appl. Opt. **37**, 1635 (1998).
[5]A. Steimacher, A. N. Medina, A. C. Bento, J. H. Rohling, and M. L. Baesso, J. Non-Cryst. Solids **348**, 240 (2004).
[6]M. L. Baesso, J. Shen, and R. D. Snook, J. Appl. Phys. **75**, 3732 (1994).
[7]A. A. Andrade, T. Catunda, I. Bodnar, J. Mura, and M. L. Baesso, Rev. Sci. Instrum. **74**, 877 (2003).
[8]M. Daimon and A. Masumura, Appl. Opt. **46**, 3881 (2007).
[9]M. Born and E. Wolf, *Principles of Optics* (Cambridge University Press, 1997).
[10]J. Proakis and D. Manolakis, *Digital Signal Processing* (Prentice-Hall, 1996).
[11]G. Abbate, A. Attanasio, U. Bernini, E. Ragozzino, and F. Somma, J. Phys. D: Appl. Phys. **9**, 1945 (1976).
[12]R. C. Weast, M. J. Astle, and W. H. Beyer, *CRC Handbook of Chemistry and Physics*, 69th ed. (CRC Press, Inc., Boca Raton, 1988).
[13]W. S. Rodney and R. J. Spindler, J. Res. Natl. Bur. Stand. **53**, 185 (1954).